

Unexpected Suppression of Fermi Level Pinning in Metal Contacts to Two-Dimensional Semiconductors MoSi_2N_4 and WSi_2N_4

Qianqian Wang^{1,2†}, Liemao Cao^{3†‡}, Shi-Jun Liang⁴, Weikang Wu^{2,5}, Guangzhao Wang^{1,2}, Ching Hua Lee⁶, Wee Liat Ong^{7,8}, Hui Ying Yang⁹, Lay Kee Ang¹, Shengyuan A. Yang^{1,2‡}, Yee Sin Ang^{1*}

1. Science, Mathematics and Technology, Singapore University of Technology and Design, Singapore 487372, Singapore.
2. Research Laboratory of Quantum Materials, Singapore University of Technology and Design, Singapore 487372, Singapore.
3. College of Physics and Electronic Engineering, Hengyang Normal University, Hengyang 421002, China.
4. National Laboratory of Solid State Microstructures, School of Physics, Collaborative Innovation Center of Advanced Microstructures, Nanjing University, Nanjing, 210093, China
5. Division of Physics and Applied Physics, School of Physical and Mathematical Sciences, Nanyang Technological University, Singapore, 637371, Singapore
6. Department of Physics, National University of Singapore, Singapore 117542, Singapore.
7. Zhejiang University-University of Illinois at Urbana-Champaign Institute (ZJU-UIUC) College of Energy Engineering, Zhejiang University, Hangzhou, Zhejiang 310027, China.
8. State Key Laboratory of Clean Energy Utilization, Zhejiang University, Hangzhou, Zhejiang, 310027, China.
9. Engineering Product Development, Singapore University of Technology and Design, Singapore 487372, Singapore.

Abstract. Metal contacts to two-dimensional (2D) semiconductors are ubiquitous in modern electronic and optoelectronic devices. Such contacts are often plagued by strong Fermi level pinning (FLP) effect which reduces the tunability of the Schottky barrier height (SBH) and degrades the performance of 2D-semiconductor-based devices. Here we show that monolayers MoSi_2N_4 and WSi_2N_4 – a recently synthesized 2D material class with exceptional mechanical and electronic properties – exhibit strongly suppressed FLP and wide-range tunable SBH when contacted by metals. An exceptionally large SBH slope parameter of $S=0.7$ is obtained. We reveal that such unexpected behavior arises from the unique morphology of MoSi_2N_4 and WSi_2N_4 . The outlying Si-N layer forms a native atomic layer that protects the semiconducting inner-core from the perturbation of metal contacts, thus suppressing the FLP. Our findings reveal the potential of MoSi_2N_4 and WSi_2N_4 monolayers as a novel 2D material platform for designing high-performance and energy-efficient 2D nanodevices.

†These authors contributed equally

‡Corresponding Author. liemao_cao@hynu.edu.cn

§Corresponding Author. shengyuan_yang@sutd.edu.sg

*Corresponding Author. yeemin_ang@sutd.edu.sg

KEYWORDS. 2D semiconductors, electrical contact, Fermi level pinning, Schottky barrier height, density functional theory simulation

Electrical contacts between metals and semiconductors are ubiquitous in modern electronic and optoelectronic devices. An interfacial potential barrier, known as the Schottky barrier (SB), is commonly formed at the metal/semiconductor interface. In electronics and optoelectronics applications, the presence of a sizable SB, typically larger than a few $k_B T$, can severely impede the charge injection efficiency¹. A SB is intimately linked to the contact resistance at the metal/semiconductor contact². Consider a contact operating in the thermionic charge injection regime^{3,4}, the contact resistance is exponentially raised by the Schottky barrier height (SBH), i.e. $R_c^{(TE)} \propto \exp(\Phi_B/k_B T)$ where Φ_B is the SBH^{1,5}. Evidently, a large Φ_B exponentially increases the R_c which, as a result, raises the power dissipation at the contact region, reduces the ‘on’ state current, I_{on} , and increases the device delay time as well as the dynamical power consumption⁶. Reducing the SBH at the metal/semiconductor contact has thus become one of the key quests towards the realization of energy-efficient and high-speed semiconductor devices⁷.

For an ideal metal/semiconductor contact, the SBH arises from the mismatch between the metal work function (W_M) and the semiconductor electron affinity E_{ea} (n -type Schottky contact) or ionization potential E_{ip} (p -type Schottky contact), and is given by the Schottky-Mott (SM) rule⁸, $\Phi_{B,e} = W_M - E_{ea}$ and $\Phi_{B,h} = E_{ip} - W_M$, respectively for n -type and p -type Schottky contact, where $\Phi_{B,e}$ and $\Phi_{B,h}$ is the electron and hole SBH of n -type and p -type Schottky contact, respectively. Due to the presence of metal/semiconductor interactions and interfacial defects, the SBH rarely follows the linear scaling with W_M as predicted by the ideal SM rule. In this case, the *modified* SM rule can be succinctly written as^{3,9,10}

$$\Phi_{Be} = S_e(W_M - E_{ea}) + c_e \quad (1)$$

$$\Phi_{Bh} = S(E_{ip} - W_M) + c_h \quad (2)$$

where the subscript ‘*e*’ and ‘*h*’ denote *n*- and *p*-type contacts, respectively, $c_{e(h)}$ is a material and contact dependent term, and $S_{e(h)} \equiv |d\Phi_{Be(h)}/dW_M|$ is the *slope parameter* – an important phenomenological parameter widely used in characterizing the deviation of the $\Phi_{Be(h)}$ vs W_M scaling from the ideal SM limit of $S = 1$. In most practical metal/semiconductor contacts, $S \ll 1$ due to the formation of metal-induced gap states, defect-induced gap states, mid-gap states and interface dipole, and/or the modifications of the electronic band structures of the semiconductor when contacted by metals^{8,10,11}. The SBH is pinned to a narrow range, an adverse effect commonly known as the *Fermi level pinning* (FLP), which poses a great challenge to the design of semiconductor electronics and optoelectronics.

Two-dimensional (2D) semiconductors, such as MoS₂ and WS₂¹², and their van der Waals heterostructures are promising in low-power electronics¹³, optoelectronics¹⁴ and neuromorphic applications^{15,16}. However, in such few-atom-thick 2D limit, 2D semiconductors continue to be plagued by FLP^{17,18}. The lack of wide-range SBH tunability has become a commonplace in many 2D semiconductors. Despite tremendous theoretical and experimental efforts, designing electrical contacts to 2D semiconductor with tunable SBH remains an ongoing challenge. Particularly, the metallization of a 2D semiconductor by the contacting metal often substantially alters the electronic structures of the heterostructure via the generation of mid-gap states^{19,20}, causing strong FLP effect that leads to a poor SBH tunability²⁰. For the vast majority of 2D semiconductors, S

is typically less than 0.4 as predicted by density functional theory (DFT) calculations^{19–33}, and are even lower in experimental measurements due to the inevitable presence of defects at the contact interface^{34–36}. To resurrect a wide-range tunable SBH in 2D semiconductors, atomically sharp van der Waals (VDW) metal/2D-semiconductor electrical contacts have been proposed³⁷. Such *VDW-type contacts* harness the weak VDW interfacial coupling to reduce the metal/semiconductor interactions, thus yielding an $S \approx 1$ approaching the ideal SM limit^{38–40}. However, as VDW-type contact often involves complex state-of-art fabrication techniques, it is constructive to search for a new class of 2D semiconductors that are *inherently* insensitive to FLP when contacted by 3D metals, so that Fermi level unpinning can be intrinsically accomplished without necessarily relying on the VDW contact paradigm.

In this work, we perform a first-principle density functional theory (DFT) investigation^{41–47} and show that, in contrary to the common knowledge that 2D semiconductors are inherently prone to strong FLP, the recently discovered *synthetic* 2D monolayers, MoSi₂N₄ and WSi₂N₄^{48,49}, exhibit strongly suppressed FLP and excellent SBH tunability without relying on the VDW-type contact engineering. The SBH is widely tunable in MoSi₂N₄ and WSi₂N₄ monolayers, reaching an exceptionally high slope parameter of $S = 0.69$ and $S = 0.77$, respectively – a value much larger than other commonly studied 2D semiconductors. The FLP suppression originates from the unique morphology of MoSi₂N₄ and WSi₂N₄ monolayers, in which the semiconducting states residing in the Mo-S or W-S inner core-layer are protected by the outlying Si-N atomic layers. Our results reveal MoSi₂N₄ and WSi₂N₄ monolayer as an unusual 2D semiconductor class with built-in atomic layer protection, thus opening up an alternative and complementary route to the VDW contact paradigm towards efficient SBH tuning and high-performance electrical contact engineering.

Electronic properties of the metal-contacted heterostructures. The 2D monolayers of MoSi_2N_4 and WSi_2N_4 (Figure 1A and 1B) belong to the family of MA_2X_4 synthetic 2D layered materials with no known 3D parent materials (M = early transition metal, A = Si or Ge, X = N, P or As). The MA_2X_4 2D material family covers a wide variety of semiconducting, metallic, insulating and magnetic phases, thus offering an exciting new platform for the exploration 2D semiconductor physics and device applications^{50–54}. MoSi_2N_4 and WSi_2N_4 monolayers are indirect band gap semiconductor with band gap values of 1.73 eV and 2.06 eV, respectively (Figure 1C and 1D), and exhibit excellent structural stability and mechanical strength⁴⁸. The MoSi_2N_4 (WSi_2N_4) monolayer is composed of a Mo-S (W-S) monolayer sandwiched by two Si-N layers. We perform first-principle DFT simulations to model the contact heterostructure composed of MoSi_2N_4 and WSi_2N_4 monolayers contacted by a large variety of metals (3D metals Sc, In, Ti, Ag, Cu, Ni, Au, Pd, Pt; 2D semimetal graphene; and 2D metal NbS_2 monolayer) with work function ranging from 3.3 eV to 6.0 eV (see *Supporting Information* for DFT simulation methods).

Our DFT calculations reveal that metal contacts to MoSi_2N_4 and WSi_2N_4 cover a large variety of contact types, including n -type Schottky contact, p -type Schottky contact, and Ohmic contact with zero SBH. The interlayer distance between the metal and 2D monolayers are less than 3 Å for Cu, Pd, Ti and Ni (see Table S1), suggesting the prevalence of non-VDW-type metal contacts. We take Au and Ti metal contacts as illustrative examples of Schottky (Figure 2) and Ohmic contacts (Figure 3), respectively (see Figure S1 for the relaxed band structures of all metal contacts calculated in this work). The lattice structures of the Au and Ti contacts to MoSi_2N_4 and WSi_2N_4 monolayers are shown in Figure 2A and Figure 3A, respectively. A closer inspection on the electronic band structures of the metal/ MoSi_2N_4 and metal/ WSi_2N_4 reveals intriguing

behaviors. The metal/semiconductor heterostructures is nearly free of mid-gap states for all metals as revealed in the projected band structures and the partial density of states (PDOS) (Figure 2B and 2E for Au Schottky contacts, and Figure 3B and 3E for Ti Ohmic contact, see also Figure S2 for the projected band structures and PDOS of other metal contacts). By projecting the 2D semiconductor electronic states onto the band structures, we find that the semiconducting bands, particularly the electronic states around the valence band maximum (VBM) and the conduction band minimum (CBM), remain intact in all metal contacts, suggesting the near absence of mid-gap states within the semiconductor band gap. For Ti contact, despite being a close contact type with exceedingly small interlayer distance of 1.75 Å and 1.78 Å, mid-gap states remain nearly absent (see PDOS in Figure 3B and 3E), which is in stark contrast to metal-contacted MoS₂ where large abundance of mid-gap states localizing in the Mo sites are created^{20,55}.

We further calculate the spatial charge density distribution around the VBM and the CBM, as well as the states between the VBM and the CBM. Intriguingly, the semiconducting electronic states are embedded deeply within the inner Mo-N (Figures 2C and 3C) and W-N core layer (Figures 2f and 3f), while the mid-gap states between the VBM and CBM are mostly located in the metals and a sparsely distributed in the outlying Si-N layers. In addition, the differential charge density ($\Delta\rho$) reveals a significant charge redistribution across the metal/semiconductor contact interface (Figure 2C and 2F; Figure 3C and 3F), signaling the presence of metal/semiconductor interactions. As $\Delta\rho$ across the contact interface is asymmetrical, the formation of interface dipole is expected to be an important factor that modifies the S parameter from the SM limit (see Figure S3 for $\Delta\rho$ of all metal contacts).

Importantly, the absence of mid-gap states in the inner core layer and the finite charge transfer at the outlying Si-N layers reveals that the metal/semiconductor interaction affects mostly the outlying S-N layers, predominantly via charge redistribution, without penetrating the semiconducting Mo-N and W-N inner cores. Here the Si-N layer serves as an encapsulating layer and plays a vital role in preserving the semiconducting characteristics of MoSi₂N₄ and WSi₂N₄ monolayers. To verify the protective effect of S-N layers, we simulate a *close contact type* of Au/MoSi₂N₄ and Au/WSi₂N₄ heterostructures^{56,57} by forcing the interlayer distance to 1.5 Å, compared to the fully relaxed value of about 3.13 Å (Figure S3). The semiconducting band structures remain well-preserved at the close-contact limit, thus confirming the robustness of the semiconducting states residing in the MoSi₂N₄ and WSi₂N₄ monolayers and the resilience against mid-gap states formation. Such unusual behavior, uniquely enabled by the *septuple-layered* morphology of MoSi₂N₄ and WSi₂N₄ monolayer, is not found in other commonly studied 2D semiconductors, such as transition metal dichalcogenides and black phosphorus, in which an external insertion layer is required to unpin the Fermi level^{58,59}.

Interface potential difference. The interface potential difference, $\Delta V = W'_M - W'_S$, where W'_S and W'_M is the work function on the semiconductor and on the metal sides of the contact heterostructures, respectively, lies typically in the range of ~ 1 eV (Fig. 4), which is consistent with that of metal-contacted 2D monolayers composed of small atom, such as graphene and hBN⁶⁰. The electronic orbitals of the outermost N atoms of the MoSi₂N₄ and WSi₂N₄ monolayers are relatively compact and hence more resilient to deformation when compared to that of the contacting metal atoms. By virtue of Pauli exclusion principle, electron density in the interfacial vacuum gap are pushed back towards the metal side, thus leading to a net transfer of electron to metal with $\Delta V > 0$ ⁶¹. The ΔV is reduced towards zero or a slightly negative value for low work

function metals of Sc and In (Figure 4A and 4B). One exception is the graphene contacts. Despite having a moderate work function of 4.91 eV, graphene/MoSi₂N₄ and graphene/WSi₂N₄ contacts exhibit $\Delta V < 0$. Here, the tug-of-war between the C and N atoms, both are first-row elements with compact electronic orbitals, lead to a slight pushed-back of electrons from the relatively more compact C atom towards the N atom, thus yielding a slightly negative ΔV .

The minimum bond length, d_{min} , is defined as the minimum distance between the contacting metal atom and the outermost N atom of MoSi₂N₄ and WSi₂N₄. In Figure 4c and 4d, the ΔV generally decreases with increasing d_{min} due to the weakening of the metal/semiconductor interactions when the metals and the 2D semiconductors are further apart. It should be noted that the Sc, Ti and Ni have relatively shorter d_{min} when compared to other metals, yet the semiconducting electronic band structures remain largely intact and the mid-gap states are strongly suppressed (see Figure S2). This is again a direct consequence of the outlying Si-N protection layer which prevents the inner core carrying the VBM and CBM electronic states from the perturbation of the contacting metals.

A tunneling potential barrier, Φ_{TB} , can form across the metal/semiconductor gap, which impedes the charge injection efficiency⁵⁵. contact heterostructures. The Φ_{TB} and the barrier width, d_{TB} is then estimated from effective electrostatic potential across the metal/semiconductor interface (see Figure S5). For both MoSi₂N₄ and WSi₂N₄ monolayers, Φ_{TB} ranges between 2.8 eV and over 5.1 eV, and the thickness d_{TB} ranges between 1.1 Å and 2 Å (see Table S1 and S2). The *electron tunneling probability* across the interface is calculated as,

$$T(\Phi_{TB}, d_{TB}) = \exp\left(-\frac{4\pi\sqrt{2m_e\Phi_{TB}}d_{TB}}{\hbar}\right) \quad (3)$$

where m_e is the free electron mass. The $T(\Phi_{TB}, d_{TB})$ calculated via Equation (3) for various metal contacts are shown in Figure 4E. For Sc, Ti and Ni, the tunneling barrier is 100% as $\Phi_{TB} = 0$. Particularly for Sc and Ti, both Φ_{TB} and Φ_B are zero in both MoSi₂N₄ and WSi₂N₄ monolayers – an indication of good Ohmic contacts with high charge injection efficiency. In contrast, the VDW type contacts, such as graphene and NbS₂ with interlayer distances greater than 3 Å, exhibit very low T of less than 2%, which suggests a low electron transparency in such VDW interfaces.

Schottky-Mott plot and the S parameter. As the semiconducting band structures of MoSi₂N₄ and WSi₂N₄, especially the CBM and VBM states, are well preserved, the electron and hole SBH can be determined from the energy differences between the CBM and the Fermi level (ε_F) of the metal/semiconductor heterostructure, and that between the ε_F and the VBM via the projected band structures and the PDOS data (see Figure S2). The Schottky-Mott plot of the metal-contacted MoSi₂N₄ and WSi₂N₄ is shown in Fig. 5. A linear fit across the 11 metal contacts reveal an remarkable slope parameter of $S_e \approx S_h = 0.69$ for MoSi₂N₄ where S_e and S_h denotes electron and hole slope parameters, and $S_e = 0.77$ and $S_h = 0.76$ for WSi₂N₄. Although being lower than that of the 2D/2D and 3D/2D VDW-type contacts^{38,39}, these S values – achieved *intrinsically* without relying on VDW-type contact engineering – are still significantly higher than that of almost all previously reported 2D semiconductors (Figure 5E), including MoS₂ monolayer and bilayer, WS₂, InSe, black and blue phosphorene, arsenene, and silicene, MoSi₂N₄ and WSi₂N₄ and spaces over a large work function range of $\Delta W_M = 2.7$ eV. Such exceptionally large S values unravel an enormous flexibility in designing metal/MoSi₂N₄ and metal/WSi₂N₄ heterostructures with custom-made SBH values useful for different device applications.

Discussion and conclusion. Due to the inevitable presence of interfacial defects and contact imperfections, the SBH and S values presented in the calculations shall serve as an upper theoretical limit useful for guiding the optimization of device designs and fabrication methods in experiments. Importantly, Ni and Ti contacts, both of which form good Ohmic contact to MoSi₂N₄ and WSi₂N₄ monolayers, are CMOS-compatible metals. Our results thus reveal a viable CMOS-compatible contact engineering strategy for the construction of high-performance 2D nanodevices. The unique septuple-layered morphology of MoSi₂N₄ and WSi₂N₄ monolayers offers a new mechanism, alternative and complementary to the VDW contact paradigm, towards Fermi level unpinning and efficient tunable SBH. Here the Si-N layers protects the inner Mo-N and W-N core layer which host the semiconducting electronic states. Even when the metal couples strongly to the 2D monolayers, such as the Sc contact (see Figure S2), the semiconducting bands remain clearly visible without substantial amount of mid-gap states formation. The large S parameter thus reveals MoSi₂N₄ and WSi₂N₄ as an intriguing 2D semiconductor class with intrinsically good SBH tunability – a much sought-after characteristic rarely found in the vast majority of 2D semiconductors. It should be emphasized that, while VDW is commonly employed to achieve tunable SBH, the metal/MoSi₂N₄ and metal/WSi₂N₄ contacts studied here exhibit a *mixture* of VDW and non-VDW types contact. This peculiar aspect reveals MoSi₂N₄ and WSi₂N₄ as a peculiar 2D semiconductor class without necessarily requiring VDW contact paradigm.

The DFT calculations presented in this work shall form a harbinger for the study of interfacial contact physics in the expansive family of MA₂X₄. Myriads of physical phenomena, such as the evolution of SBH and FLP with different number of layers⁶², the nature of 2D/2D and 2D/3D contacts for the other semiconducting members of the expansive MA₂X₄ family, the design of MA₂X₄ contact or heterostructures that can facilitate unusual *non-charge* transport, such as

spin and valley transport⁶³, or neuromorphic device operations^{15,16}, remain to be explored. Future computational and experimental studies of 2D/2D and 2D/3D MA₂X₄ contacts and heterostructures shall bring more surprises and new insights on the fundamental interface physics and the applied engineering of MA₂X₄ -based heterostructures and devices⁶⁴⁻⁶⁶.

REFERENCES

- (1) Allain, A.; Kang, J.; Banerjee, K.; Kis, A. Electrical Contacts to Two-Dimensional Semiconductors. *Nat. Mater.* **2015**, *14* (12), 1195–1205.
<https://doi.org/10.1038/nmat4452>.
- (2) Chhowalla, M.; Jena, D.; Zhang, H. Two-Dimensional Semiconductors for Transistors. *Nat. Rev. Mater.* **2016**, *1* (11), 16052. <https://doi.org/10.1038/natrevmats.2016.52>.
- (3) Sze, S. M.; Ng, K. K. *Physics of Semiconductor Devices*, 3rd Editio.; John Wiley & Sons Ltd: USA, 2006.
- (4) Chang, C. Y.; Fang, Y. K.; Sze, S. M. Specific Contact Resistance of Metal-Semiconductor Barriers. *Solid. State. Electron.* **1971**, *14* (7), 541–550.
[https://doi.org/10.1016/0038-1101\(71\)90129-8](https://doi.org/10.1016/0038-1101(71)90129-8).
- (5) Ang, Y. S.; Yang, H. Y.; Ang, L. K. Universal Scaling Laws in Schottky Heterostructures Based on Two-Dimensional Materials. *arXiv*. 2018.
- (6) Fiori, G.; Bonaccorso, F.; Iannaccone, G.; Palacios, T.; Neumaier, D.; Seabaugh, A.; Banerjee, S. K.; Colombo, L. Electronics Based on Two-Dimensional Materials. *Nat. Nanotechnol.* **2014**, *9* (10), 768–779. <https://doi.org/10.1038/nnano.2014.207>.
- (7) Ferrari, A. C.; Bonaccorso, F.; Fal'ko, V.; Novoselov, K. S.; Roche, S.; Bøggild, P.; Borini, S.; Koppens, F. H. L.; Palermo, V.; Pugno, N.; Garrido, J. A.; Sordan, R.; Bianco, A.; Ballerini, L.; Prato, M.; Lidorikis, E.; Kivioja, J.; Marinelli, C.; Ryhänen, T.; Morpurgo, A.; Coleman, J. N.; Nicolosi, V.; Colombo, L.; Fert, A.; Garcia-Hernandez, M.; Bachtold, A.; Schneider, G. F.; Guinea, F.; Dekker, C.; Barbone, M.; Sun, Z.; Galiotis, C.; Grigorenko, A. N.; Konstantatos, G.; Kis, A.; Katsnelson, M.; Vandersypen, L.; Loiseau, A.; Morandi, V.; Neumaier, D.; Treossi, E.; Pellegrini, V.; Polini, M.;

- Tredicucci, A.; Williams, G. M.; Hee Hong, B.; Ahn, J.-H.; Min Kim, J.; Zirath, H.; van Wees, B. J.; van der Zant, H.; Occhipinti, L.; Di Matteo, A.; Kinloch, I. A.; Seyller, T.; Quesnel, E.; Feng, X.; Teo, K.; Rupesinghe, N.; Hakonen, P.; Neil, S. R. T.; Tannock, Q.; Löfwander, T.; Kinaret, J. Science and Technology Roadmap for Graphene, Related Two-Dimensional Crystals, and Hybrid Systems. *Nanoscale* **2015**, *7* (11), 4598–4810.
<https://doi.org/10.1039/C4NR01600A>.
- (8) Tung, R. T. The Physics and Chemistry of the Schottky Barrier Height. *Appl. Phys. Rev.* **2014**, *1* (1), 011304. <https://doi.org/10.1063/1.4858400>.
- (9) Cowley, A. M.; Sze, S. M. Surface States and Barrier Height of Metal-Semiconductor Systems. *J. Appl. Phys.* **1965**, *36* (10), 3212–3220. <https://doi.org/10.1063/1.1702952>.
- (10) Tung, R. T. Chemical Bonding and Fermi Level Pinning at Metal-Semiconductor Interfaces. *Phys. Rev. Lett.* **2000**, *84* (26), 6078–6081.
<https://doi.org/10.1103/PhysRevLett.84.6078>.
- (11) Bardeen, J. Surface States and Rectification at a Metal Semi-Conductor Contact. *Phys. Rev.* **1947**, *71* (10), 717–727. <https://doi.org/10.1103/PhysRev.71.717>.
- (12) Manzeli, S.; Ovchinnikov, D.; Pasquier, D.; Yazyev, O. V.; Kis, A. 2D Transition Metal Dichalcogenides. *Nat. Rev. Mater.* **2017**, *2* (8), 17033.
<https://doi.org/10.1038/natrevmats.2017.33>.
- (13) Fiori, G.; Bonaccorso, F.; Iannaccone, G.; Palacios, T.; Neumaier, D.; Seabaugh, A.; Banerjee, S. K.; Colombo, L. Electronics Based on Two-Dimensional Materials. *Nat. Nanotechnol.* **2014**, *9* (10), 768–779. <https://doi.org/10.1038/nnano.2014.207>.
- (14) Liang, S.; Cheng, B.; Cui, X.; Miao, F. Van Der Waals Heterostructures for High-Performance Device Applications: Challenges and Opportunities. *Adv. Mater.* **2019**,

1903800. <https://doi.org/10.1002/adma.201903800>.
- (15) Pan, C.; Wang, C.-Y.; Liang, S.-J.; Wang, Y.; Cao, T.; Wang, P.; Wang, C.; Wang, S.; Cheng, B.; Gao, A.; Liu, E.; Watanabe, K.; Taniguchi, T.; Miao, F. Reconfigurable Logic and Neuromorphic Circuits Based on Electrically Tunable Two-Dimensional Homojunctions. *Nat. Electron.* **2020**, *3* (7), 383–390. <https://doi.org/10.1038/s41928-020-0433-9>.
- (16) Wang, M.; Cai, S.; Pan, C.; Wang, C.; Lian, X.; Zhuo, Y.; Xu, K.; Cao, T.; Pan, X.; Wang, B.; Liang, S.-J.; Yang, J. J.; Wang, P.; Miao, F. Robust Memristors Based on Layered Two-Dimensional Materials. *Nat. Electron.* **2018**, *1* (2), 130–136. <https://doi.org/10.1038/s41928-018-0021-4>.
- (17) Kim, C.; Moon, I.; Lee, D.; Choi, M. S.; Ahmed, F.; Nam, S.; Cho, Y.; Shin, H.-J.; Park, S.; Yoo, W. J. Fermi Level Pinning at Electrical Metal Contacts of Monolayer Molybdenum Dichalcogenides. *ACS Nano* **2017**, *11* (2), 1588–1596. <https://doi.org/10.1021/acsnano.6b07159>.
- (18) Xu, Y.; Cheng, C.; Du, S.; Yang, J.; Yu, B.; Luo, J.; Yin, W.; Li, E.; Dong, S.; Ye, P.; Duan, X. Contacts between Two- and Three-Dimensional Materials: Ohmic, Schottky, and p – n Heterojunctions. *ACS Nano* **2016**, *10* (5), 4895–4919. <https://doi.org/10.1021/acsnano.6b01842>.
- (19) Kang, J.; Liu, W.; Sarkar, D.; Jena, D.; Banerjee, K. Computational Study of Metal Contacts to Monolayer Transition-Metal Dichalcogenide Semiconductors. *Phys. Rev. X* **2014**, *4* (3), 031005. <https://doi.org/10.1103/PhysRevX.4.031005>.
- (20) Gong, C.; Colombo, L.; Wallace, R. M.; Cho, K. The Unusual Mechanism of Partial Fermi Level Pinning at Metal–MoS₂ Interfaces. *Nano Lett.* **2014**, *14* (4), 1714–1720.

- <https://doi.org/10.1021/nl403465v>.
- (21) Guo, Y.; Robertson, J. Band Structure, Band Offsets, Substitutional Doping, and Schottky Barriers of Bulk and Monolayer InSe. *Phys. Rev. Mater.* **2017**, *1* (4), 044004.
<https://doi.org/10.1103/PhysRevMaterials.1.044004>.
- (22) Shen, T.; Ren, J.-C.; Liu, X.; Li, S.; Liu, W. Van Der Waals Stacking Induced Transition from Schottky to Ohmic Contacts: 2D Metals on Multilayer InSe. *J. Am. Chem. Soc.* **2019**, *141* (7), 3110–3115. <https://doi.org/10.1021/jacs.8b12212>.
- (23) Gao, N.; Zhou, S.; Liu, N.; Bai, Y.; Zhao, J. Selecting Electrode Materials for Monolayer ReS₂ with an Ohmic Contact. *J. Mater. Chem. C* **2018**, *6* (25), 6764–6770.
<https://doi.org/10.1039/C8TC02116C>.
- (24) Tang, H.; Shi, B.; Pan, Y.; Li, J.; Zhang, X.; Yan, J.; Liu, S.; Yang, J.; Xu, L.; Yang, J.; Wu, M.; Lu, J. Schottky Contact in Monolayer WS₂ Field-Effect Transistors. *Adv. Theory Simulations* **2019**, *2* (5), 1900001. <https://doi.org/10.1002/adts.201900001>.
- (25) Wang, Y.; Yang, R. X.; Quhe, R.; Zhong, H.; Cong, L.; Ye, M.; Ni, Z.; Song, Z.; Yang, J.; Shi, J.; Li, J.; Lu, J. Does P-Type Ohmic Contact Exist in WSe₂–Metal Interfaces? *Nanoscale* **2016**, *8* (2), 1179–1191. <https://doi.org/10.1039/C5NR06204G>.
- (26) Zhong, H.; Quhe, R.; Wang, Y.; Ni, Z.; Ye, M.; Song, Z.; Pan, Y.; Yang, J.; Yang, L.; Lei, M.; Shi, J.; Lu, J. Interfacial Properties of Monolayer and Bilayer MoS₂ Contacts with Metals: Beyond the Energy Band Calculations. *Sci. Rep.* **2016**, *6* (1), 21786.
<https://doi.org/10.1038/srep21786>.
- (27) Guo, Y.; Liu, D.; Robertson, J. 3D Behavior of Schottky Barriers of 2D Transition-Metal Dichalcogenides. *ACS Appl. Mater. Interfaces* **2015**, *7* (46), 25709–25715.
<https://doi.org/10.1021/acsami.5b06897>.

- (28) Pan, Y.; Wang, Y.; Ye, M.; Quhe, R.; Zhong, H.; Song, Z.; Peng, X.; Yu, D.; Yang, J.; Shi, J.; Lu, J. Monolayer Phosphorene–Metal Contacts. *Chem. Mater.* **2016**, *28* (7), 2100–2109. <https://doi.org/10.1021/acs.chemmater.5b04899>.
- (29) Pan, Y.; Dan, Y.; Wang, Y.; Ye, M.; Zhang, H.; Quhe, R.; Zhang, X.; Li, J.; Guo, W.; Yang, L.; Lu, J. Schottky Barriers in Bilayer Phosphorene Transistors. *ACS Appl. Mater. Interfaces* **2017**, *9* (14), 12694–12705. <https://doi.org/10.1021/acsami.6b16826>.
- (30) Zhang, X.; Pan, Y.; Ye, M.; Quhe, R.; Wang, Y.; Guo, Y.; Zhang, H.; Dan, Y.; Song, Z.; Li, J.; Yang, J.; Guo, W.; Lu, J. Three-Layer Phosphorene-Metal Interfaces. *Nano Res.* **2018**, *11* (2), 707–721. <https://doi.org/10.1007/s12274-017-1680-6>.
- (31) Li, J.; Sun, X.; Xu, C.; Zhang, X.; Pan, Y.; Ye, M.; Song, Z.; Quhe, R.; Wang, Y.; Zhang, H.; Guo, Y.; Yang, J.; Pan, F.; Lu, J. Electrical Contacts in Monolayer Blue Phosphorene Devices. *Nano Res.* **2018**, *11* (4), 1834–1849. <https://doi.org/10.1007/s12274-017-1801-2>.
- (32) Zhang, H.; Xiong, J.; Ye, M.; Li, J.; Zhang, X.; Quhe, R.; Song, Z.; Yang, J.; Zhang, Q.; Shi, B.; Yan, J.; Guo, W.; Robertson, J.; Wang, Y.; Pan, F.; Lu, J. Interfacial Properties of Monolayer Antimonene Devices. *Phys. Rev. Appl.* **2019**, *11* (6), 064001. <https://doi.org/10.1103/PhysRevApplied.11.064001>.
- (33) Yan, J.; Zhang, X.; Pan, Y.; Li, J.; Shi, B.; Liu, S.; Yang, J.; Song, Z.; Zhang, H.; Ye, M.; Quhe, R.; Wang, Y.; Yang, J.; Pan, F.; Lu, J. Monolayer Tellurene–Metal Contacts. *J. Mater. Chem. C* **2018**, *6* (23), 6153–6163. <https://doi.org/10.1039/C8TC01421C>.
- (34) Liu, Y.; Guo, J.; Zhu, E.; Liao, L.; Lee, S.-J.; Ding, M.; Shakir, I.; Gambin, V.; Huang, Y.; Duan, X. Approaching the Schottky-Mott Limit in van Der Waals Metal-Semiconductor Junctions. *Nature* **2018**, *557* (7707), 696–700. <https://doi.org/10.1038/s41586-018-0129-8>.
- (35) Das, S.; Chen, H.-Y.; Penumatcha, A. V.; Appenzeller, J. High Performance Multilayer

- MoS 2 Transistors with Scandium Contacts. *Nano Lett.* **2013**, *13* (1), 100–105.
<https://doi.org/10.1021/nl303583v>.
- (36) Lv, C.; Yan, W.; Shieh, T.-H.; Zhao, Y.; Wu, G.; Zhao, Y.; Lv, Y.; Zhang, D.; Chen, Y.; Arora, S. K.; Ó Coileáin, C.; Chang, C.-R.; Cheng, H. H.; Hung, K.-M.; Wu, H.-C. Electrical Contact Barriers between a Three-Dimensional Metal and Layered SnS 2. *ACS Appl. Mater. Interfaces* **2020**, *12* (13), 15830–15836.
<https://doi.org/10.1021/acsami.9b21996>.
- (37) Liu, Y.; Huang, Y.; Duan, X. Van Der Waals Integration before and beyond Two-Dimensional Materials. *Nature* **2019**, *567* (7748), 323–333.
<https://doi.org/10.1038/s41586-019-1013-x>.
- (38) Liu, Y.; Stradins, P.; Wei, S.-H. Van Der Waals Metal-Semiconductor Junction: Weak Fermi Level Pinning Enables Effective Tuning of Schottky Barrier. *Sci. Adv.* **2016**, *2* (4), e1600069. <https://doi.org/10.1126/sciadv.1600069>.
- (39) Liu, Y.; Guo, J.; Zhu, E.; Liao, L.; Lee, S.-J.; Ding, M.; Shakir, I.; Gambin, V.; Huang, Y.; Duan, X. Approaching the Schottky–Mott Limit in van Der Waals Metal–Semiconductor Junctions. *Nature* **2018**, *557* (7707), 696–700. <https://doi.org/10.1038/s41586-018-0129-8>.
- (40) Wang, Y.; Kim, J. C.; Wu, R. J.; Martinez, J.; Song, X.; Yang, J.; Zhao, F.; Mkhoyan, A.; Jeong, H. Y.; Chhowalla, M. Van Der Waals Contacts between Three-Dimensional Metals and Two-Dimensional Semiconductors. *Nature* **2019**, *568* (7750), 70–74.
<https://doi.org/10.1038/s41586-019-1052-3>.
- (41) Kresse, G.; Hafner, J. Ab Initio Molecular Dynamics for Liquid Metals. *Phys. Rev. B* **1993**, *47* (1), 558–561. <https://doi.org/10.1103/PhysRevB.47.558>.
- (42) Kresse, G.; Furthmüller, J. Efficiency of Ab-Initio Total Energy Calculations for Metals

- and Semiconductors Using a Plane-Wave Basis Set. *Comput. Mater. Sci.* **1996**, *6* (1), 15–50. [https://doi.org/10.1016/0927-0256\(96\)00008-0](https://doi.org/10.1016/0927-0256(96)00008-0).
- (43) Blöchl, P. E. Projector Augmented-Wave Method. *Phys. Rev. B* **1994**, *50* (24), 17953–17979. <https://doi.org/10.1103/PhysRevB.50.17953>.
- (44) Joubert, D. From Ultrasoft Pseudopotentials to the Projector Augmented-Wave Method. *Phys. Rev. B - Condens. Matter Mater. Phys.* **1999**, *59* (3), 1758–1775. <https://doi.org/10.1103/PhysRevB.59.1758>.
- (45) Perdew, J. P.; Burke, K.; Ernzerhof, M. Generalized Gradient Approximation Made Simple. *Phys. Rev. Lett.* **1996**, *77* (18), 3865–3868. <https://doi.org/10.1103/PhysRevLett.77.3865>.
- (46) Monkhorst, H. J.; Pack, J. D. Special Points for Brillouin-Zone Integrations. *Phys. Rev. B* **1976**, *13* (12). <https://doi.org/10.1103/PhysRevB.13.5188>.
- (47) Grimme, S.; Antony, J.; Ehrlich, S.; Krieg, H. A Consistent and Accurate Ab Initio Parametrization of Density Functional Dispersion Correction (DFT-D) for the 94 Elements H-Pu. *J. Chem. Phys.* **2010**, *132* (15). <https://doi.org/10.1063/1.3382344>.
- (48) Hong, Y.-L.; Liu, Z.; Wang, L.; Zhou, T.; Ma, W.; Xu, C.; Feng, S.; Chen, L.; Chen, M.-L.; Sun, D.-M.; Chen, X.-Q.; Cheng, H.-M.; Ren, W. Chemical Vapor Deposition of Layered Two-Dimensional MoSi₂N₄ Materials. *Science* (80-.). **2020**, *369* (6504), 670–674. <https://doi.org/10.1126/science.abb7023>.
- (49) Novoselov, K. S. Discovery of 2D van Der Waals Layered MoSi₂N₄ Family. *Natl. Sci. Rev.* **2020**. <https://doi.org/10.1093/nsr/nwaa190>.
- (50) Cao, L.; Zhou, G.; Ang, L. K.; Ang, Y. S. Two-Dimensional van Der Waals Electrical Contact to Monolayer MoSi₂N₄. **2020**.

- (51) Zhong, H.; Xiong, W.; Lv, P.; Yu, J.; Yuan, S. Strain-Induced Semiconductor to Metal Transition in MA₂Z₄ Bilayers. **2020**.
- (52) Kang, L.; Lin, Z. Second Harmonic Generation of MoSi₂N₄ Layer. **2020**.
- (53) Bafekry, A.; Faraji, M.; Hoat, D. M.; Fadlallah, M. M.; Shahrokhi, M.; Shojaei, F.; Gogova, D.; Ghergherehchi, M. MoSi₂N₄ Single-Layer: A Novel Two-Dimensional Material with Outstanding Mechanical, Thermal, Electronic, Optical, and Photocatalytic Properties. **2020**.
- (54) Li, S.; Wu, W.; Feng, X.; Guan, S.; Feng, W.; Yao, Y.; Yang, S. A Valley-Dependent Properties of Monolayer MoSi₂N₄, WSi₂N₄ and MoSi₂As₄. **2020**.
- (55) Popov, I.; Seifert, G.; Tománek, D. Designing Electrical Contacts to MoS₂ Monolayers: A Computational Study. *Phys. Rev. Lett.* **2012**, *108* (15), 156802.
<https://doi.org/10.1103/PhysRevLett.108.156802>.
- (56) Kong, L.; Zhang, X.; Tao, Q.; Zhang, M.; Dang, W.; Li, Z.; Feng, L.; Liao, L.; Duan, X.; Liu, Y. Doping-Free Complementary WSe₂ Circuit via van Der Waals Metal Integration. *Nat. Commun.* **2020**, *11* (1), 1866. <https://doi.org/10.1038/s41467-020-15776-x>.
- (57) Lau, C. S.; Chee, J. Y.; Ang, Y. S.; Tong, S. W.; Cao, L.; Ooi, Z.-E.; Wang, T.; Ang, L. K.; Wang, Y.; Chhowalla, M.; Goh, K. E. J. Quantum Transport in Two-Dimensional WS₂ with High-Efficiency Carrier Injection through Indium Alloy Contacts. *ACS Nano* **2020**, *14* (10). <https://doi.org/10.1021/acsnano.0c05915>.
- (58) Farmanbar, M.; Brocks, G. Ohmic Contacts to 2D Semiconductors through van Der Waals Bonding. *Adv. Electron. Mater.* **2016**, *2* (4), 1500405.
<https://doi.org/10.1002/aelm.201500405>.
- (59) Kim, G.-S.; Kim, S.-H.; Park, J.; Han, K. H.; Kim, J.; Yu, H.-Y. Schottky Barrier Height

- Engineering for Electrical Contacts of Multilayered MoS₂ Transistors with Reduction of Metal-Induced Gap States. *ACS Nano* **2018**, *12* (6), 6292–6300.
<https://doi.org/10.1021/acsnano.8b03331>.
- (60) Farmanbar, M.; Brocks, G. First-Principles Study of van Der Waals Interactions and Lattice Mismatch at MoS₂/Metal Interfaces. *Phys. Rev. B* **2016**, *93* (8), 085304.
<https://doi.org/10.1103/PhysRevB.93.085304>.
- (61) Bokdam, M.; Brocks, G.; Kelly, P. J. Large Potential Steps at Weakly Interacting Metal-Insulator Interfaces. *Phys. Rev. B* **2014**, *90* (20), 201411.
<https://doi.org/10.1103/PhysRevB.90.201411>.
- (62) Wang, Q.; Shao, Y.; Gong, P.; Shi, X. Metal–2D Multilayered Semiconductor Junctions: Layer-Number Dependent Fermi-Level Pinning. *J. Mater. Chem. C* **2020**, *8* (9), 3113–3119. <https://doi.org/10.1039/C9TC06331E>.
- (63) Chen, J.-R.; Odenthal, P. M.; Swartz, A. G.; Floyd, G. C.; Wen, H.; Luo, K. Y.; Kawakami, R. K. Control of Schottky Barriers in Single Layer MoS₂ Transistors with Ferromagnetic Contacts. *Nano Lett.* **2013**, *13* (7), 3106–3110.
<https://doi.org/10.1021/nl4010157>.
- (64) Akinwande, D.; Huyghebaert, C.; Wang, C.-H.; Serna, M. I.; Goossens, S.; Li, L.-J.; Wong, H.-S. P.; Koppens, F. H. L. Graphene and Two-Dimensional Materials for Silicon Technology. *Nature* **2019**, *573* (7775), 507–518. <https://doi.org/10.1038/s41586-019-1573-9>.
- (65) Lanza, M.; Smets, Q.; Huyghebaert, C.; Li, L.-J. Yield, Variability, Reliability, and Stability of Two-Dimensional Materials Based Solid-State Electronic Devices. *Nat. Commun.* **2020**, *11* (1), 5689. <https://doi.org/10.1038/s41467-020-19053-9>.

- (66) Li, M.-Y.; Su, S.-K.; Wong, H.-S. P.; Li, L.-J. How 2D Semiconductors Could Extend Moore's Law. *Nature* **2019**, *567* (7747), 169–170. <https://doi.org/10.1038/d41586-019-00793-8>.

ASSOCIATED CONTENTS

Supporting Information

Methods of DFT simulations; relaxed lattice structures; projected band structures and projected density of states; effective potential; differential charge density; tables of key parameters calculated for the metal contacts.

AUTHOR INFORMATION

Corresponding Authors

Liemao Cao – College of Physics and Electronic Engineering, Hengyang Normal University, Hengyang 421002, China

Email: liemao_cao@hynu.edu.cn

Shengyuan Yang – Science, Mathematics and Technology & Research Laboratory of Quantum Materials, Singapore University of Technology and Design, Singapore 487372;

Email: shengyuan_yang@sutd.edu.sg

Yee Sin Ang – Science, Mathematics and Technology, Singapore University of Technology and Design, Singapore 487372;

Email: yeemin_ang@sutd.edu.sg

Notes

The authors declare no competing interests.

ACKNOWLEDGMENTS

This work is supported by SUTD Start-Up Grant, Singapore Ministry of Education (MOE) Tier 2 Grant (No. 2018-T2-1-007), USA Office of Naval Research Global (ONRG) Grant (No. N62909-19-1-2047) and SUTD-ZJU IDEA Visiting Professor Grant (SUTD-ZJU (VP) 202001). Q.W. is supported by SUTD PhD Fellowship. S.A.Y acknowledges the support of Singapore MOE AcRF Tier 2 (Grant No. MOE2017-T2-2-108). C.H.L. is supported by Singapore Ministry of Education Academic Research Fund Tier I (WBS No. R-144-000-435-133).

Figures

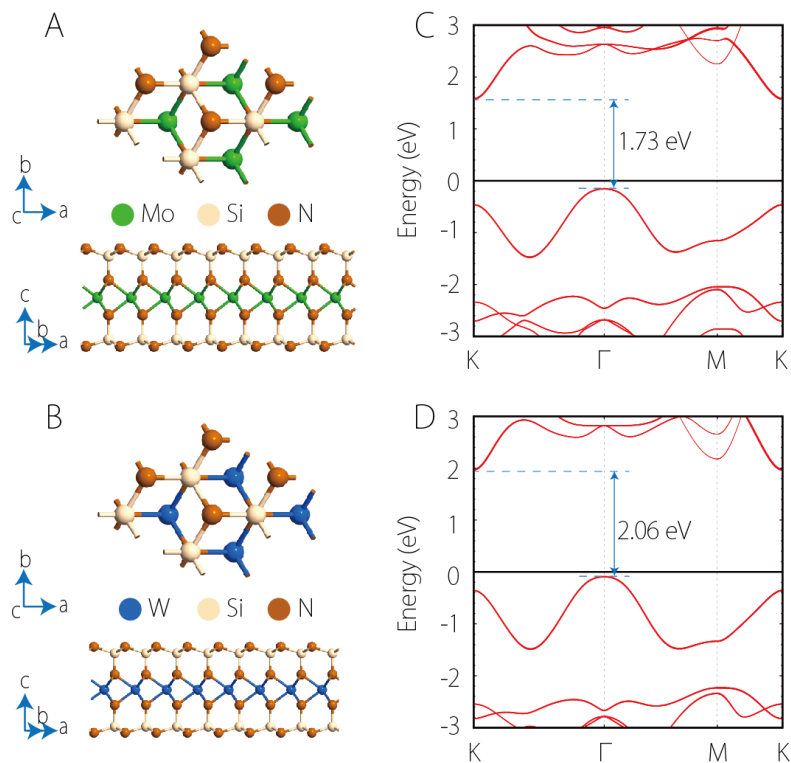


Figure 1. Crystal and electronic band structures of isolated MoSi₂N₄ and WSi₂N₄ monolayers, and a comparison of the slope parameter (*S*) for various 2D semiconductors.

Top and side view of (A) MoSi₂N₄ monolayer and (B) WSi₂N₄ monolayer. Electronic band structures of isolated (C) MoSi₂N₄ and (D) WSi₂N₄ monolayers.

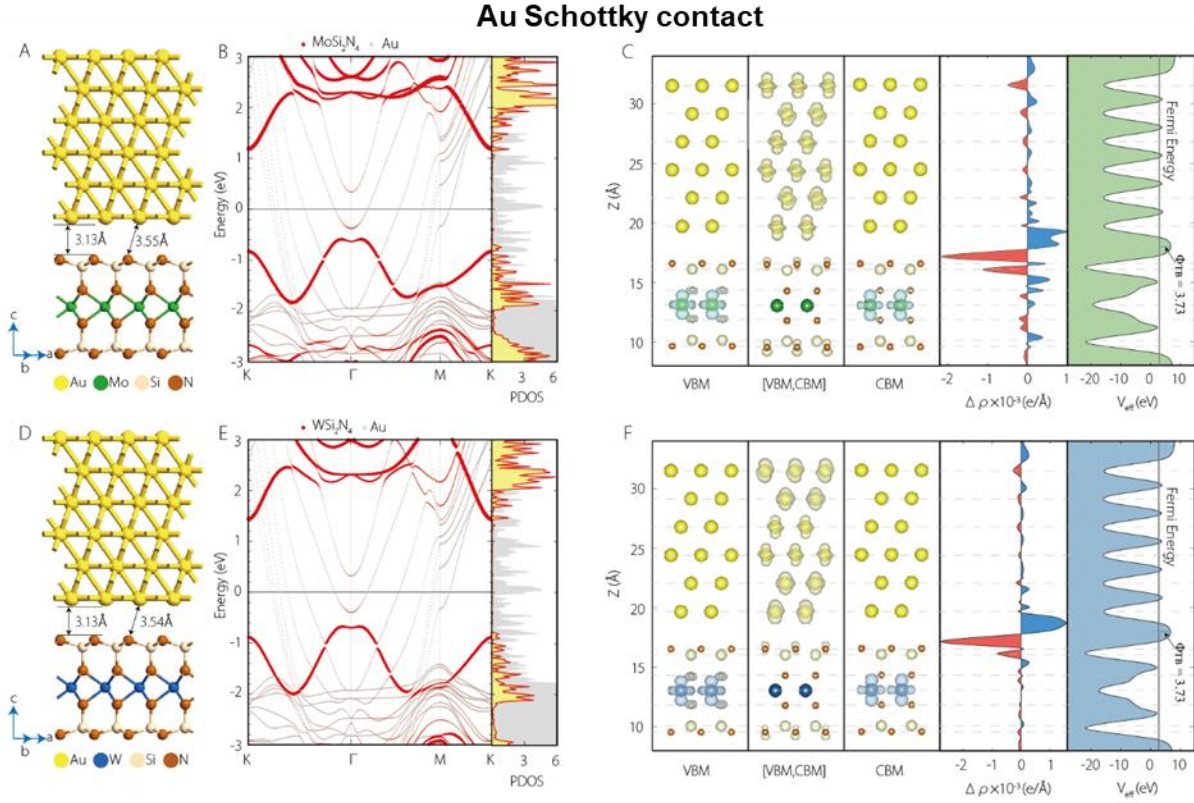


Figure 2. Schottky contacts of Au/MoSi₂N₄ and Au/WSi₂N₄ - Structural and electronic properties of. (A) The contact is composed of 6 layers of Au atoms contacting the MoSi₂N₄ monolayer. The interlayer distance is 3.13 Å and the minimum distance between Au and N atoms is 3.55 Å. (B) the projected electronic band structure and the density of states of Au/MoSi₂N₄ contact. (C) The panels, from left to right, show the spatial charge density distribution of VBM states, mid-gap states between VBM and CBM, and the CBM states, the differential charge density, and the electrostatic potential profile across the heterostructures. (D), (E) and (F), same as (A), (B) and (C), respectively, for Au/WSi₂N₄ contact. The interlayer distance is 3.13 Å and the minimum distance between Au and N atoms is 3.54 Å.

CMOS-compatible Ti Ohmic contact

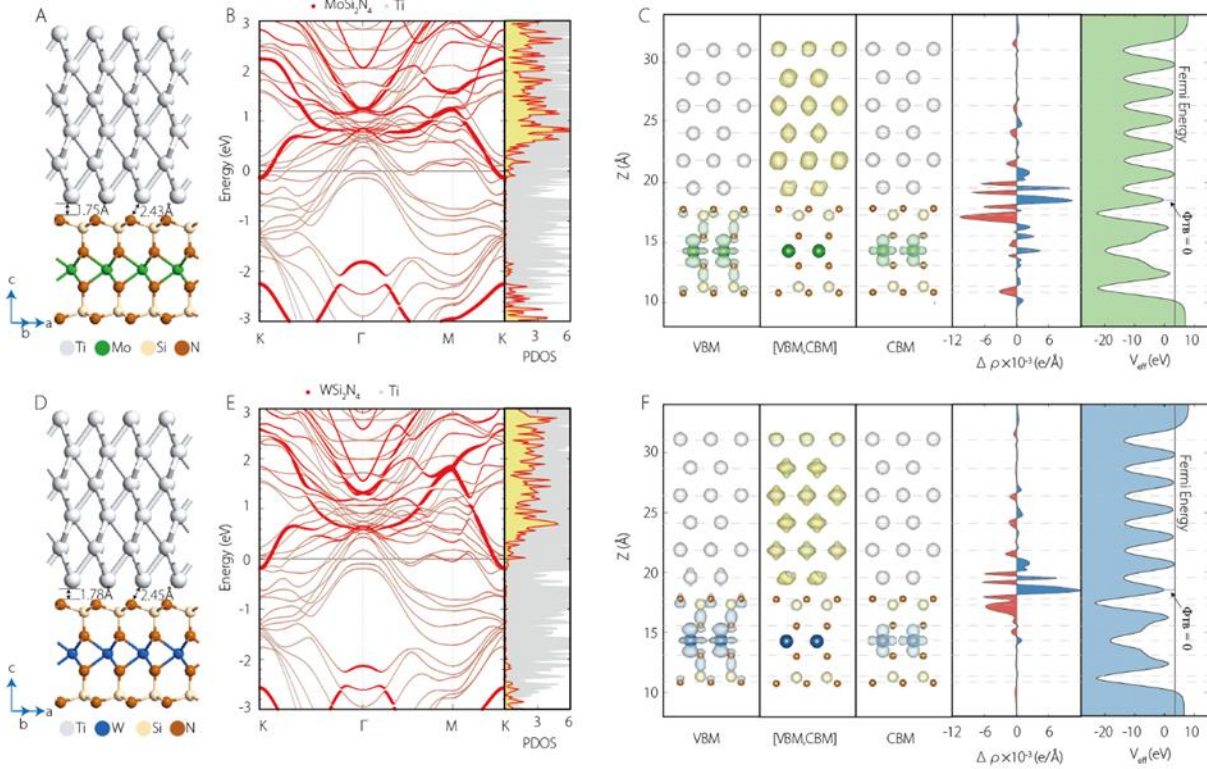


Figure 3. Ohmic contacts of Ti/MoSi₂N₄ and Ti/WSi₂N₄ Ohmic contacts: Structural and electronic properties. (A) The contact is composed of 6 layers of Ti atoms contacting the MoSi₂N₄ monolayer. The interlayer distance is 1.75 Å and the minimum distance between Ti and N atoms is 2.43 Å. (B) the projected electronic band structure and the density of states of Ti/MoSi₂N₄ contact. (C) The panels, from left to right, show the spatial charge density distribution of VBM states, mid-gap states between VBM and CBM, and the CBM states, the differential charge density, and the electrostatic potential profile across the heterostructures. (D), (E) and (F), same as (A), (B) and (C), respectively, for Ti/WSi₂N₄ contact. The interlayer distance is 1.78 Å and the minimum distance between Ti and N atoms is 2.45 Å.

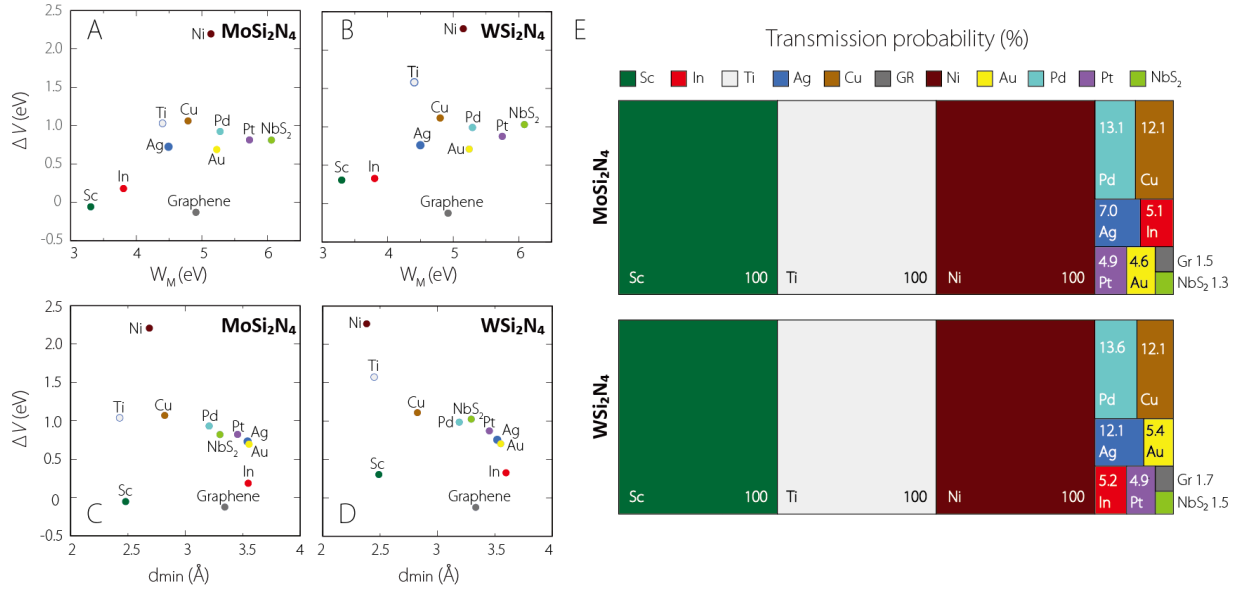


Figure 4. Interface potential difference (ΔV) and transmission probability for metal-contacted MoSi₂N₄ and WSi₂N₄ monolayers. (A) and (B) shows the isolated metal work function (W_M) dependence of ΔV for MoSi₂N₄ and WSi₂N₄, respectively. (C) and (D) shows the minimum bond length (d_{min}) dependence of ΔV for MoSi₂N₄ and WSi₂N₄, respectively. (E) Transmission probability of metal/MoSi₂N₄ and metal/WSi₂N₄, respectively.

Supplementary Materials

Fig. S1. Relaxed lattice structures of metal/MoSi₂N₄ and metal/WSi₂N₄ heterostructures.

Fig. S2. Electronic band structures and projected density of states (PDOS) of metal-contacted MoSi₂N₄ (top panel) and WSi₂N₄ (bottom panel) heterostructures.

Fig. S3. Close contact of Au/MoSi₂N₄ and Au/WSi₂N₄ heterostructures.

Fig. S4. The differential charge density ($\Delta\rho$) of metal-contacted MoSi₂N₄ (top panel) and WSi₂N₄ (bottom panel) heterostructures.

Fig. S5. The effective electrostatic potential (V_{eff}) of metal-contacted MoSi₂N₄ (top panel) and WSi₂N₄ (bottom panel) heterostructures.

Table S1. DFT calculated interfacial quantities for metal/MoSi₂N₄ heterostructures.

Table S2. DFT calculated interfacial quantities for metal/WSi₂N₄ heterostructures.

Table of Content (ToC) Image

